Published in final edited form as:
Nat Med. 2016 January ; 22(1): 54–63. doi:10.1038/nm.3983.

Parkinson's disease-associated mutant VPS35 causes mitochondrial dysfunction by recycling DLP1 complexes

Wenzhang Wang[#1], **Xinglong Wang**[#1], **Hisashi Fujioka**[2], **Charles Hoppel**[3,4], **Alan L. Whone**[5], **Maeve A. Caldwell**[6], **Peter J. Cullen**[7], **Jun Liu**[8], and **Xiongwei Zhu**[1]

[1]Department of Pathology, Case Western Reserve University, Cleveland, OH, USA

[2]Electron Microscopy Core Facility, Case Western Reserve University, Cleveland, Ohio, USA

[3]Department of Pharmacology, Case Western Reserve University, Cleveland, OH, USA

[4]Center for Mitochondrial Diseases, Department of Medicine, Case Western Reserve University, Cleveland, OH, USA

[5]Institute of Clinical Neurosciences, Southmead Hospital, University of Bristol, Bristol, UK

[6]Trinity College Institute for Neuroscience, Trinity College Dublin, Dublin, Ireland

[7]The Henry Wellcome Integrated Signaling Laboratories, School of Biochemistry, University of Bristol, Bristol, UK

[8]Department of Neurology & Institute of Neurology, Ruijin Hospital, Shanghai Jiao Tong University School of Medicine, Shanghai, China

[#] These authors contributed equally to this work.

Abstract

Mitochondrial dysfunction represents a critical step during the pathogenesis of Parkinson disease (PD) and increasing evidence suggests abnormal mitochondrial dynamics and quality control as important underlying mechanisms. The *VPS35* gene, encoding a key component of the retromer complex, is the third autosomal-dominant gene associated with PD. However, how VPS35 mutations may lead to neurodegeneration remains unclear. Here we demonstrate that PD-associated VPS35 mutations caused mitochondrial fragmentation and cell death in cultured neurons *in vitro*, in mouse substantia nigra neurons *in vivo*, and in human fibroblasts from PD patient bearing the D620N mutation. VPS35-induced mitochondrial deficits and neuronal dysfunction could be prevented by inhibition of mitochondrial fission. VPS35 mutation caused

Correspondence should be addressed to X.Z. (xiongwei.zhu@case.edu), J.L. (jly0520@hotmail.com) or X.W. (xinglong.wang@case.edu).

Author contributions

X.Z. and X.W. conceived and directed the project, interpreted results and wrote the manuscript. W.W. and X.W. designed and carried out experiments, analyzed results, generated the figures. H.F. helped with electron microscopy (EM) and immuno-EM study. C.H. helped with measurement of bioenergetics, A.L.W, M.A.C. and P.J.C. contributed fibroblasts from PD subject bearing D620N VPS35 mutation and provided feedback on the manuscript. J.L. contributed to the conception of the project, design of experiments and interpretation of results and provided feedback on the manuscript.

Competing financial interests

The authors declare no competing financial interests.

Europe PMC Funders Author Manuscripts

increased interactions with DLP1 which enhanced mitochondrial DLP1 complex turnover via mitochondria-derived vesicles-dependent trafficking to lysosomes for degradation. Importantly, oxidative stress increased the VPS35–DLP1 interaction which was also increased in the brains of sporadic PD cases. These results revealed a novel cellular mechanism for the involvement of VPS35 in mitochondrial fission, dysregulation of which is likely involved in the pathogenesis of familial, and possibly sporadic, PD.

Introduction

Mitochondria are dynamic organelles that undergo continual fission and fusion regulated by large GTPases such as dynamin like protein 1 (DLP1) for fission and mitofusin 2 (Mfn2) for fusion[1]. Unopposed mitochondrial fission or fusion causes human neurological diseases and is increasingly implicated in neurodegenerative diseases including Parkinson's disease (PD)[2-4]. Proteins encoded by previously identified genes associated with familial PD, including α-synuclein, PTEN-induced putative kinase 1 (PINK1), PARKIN, leucine-rich repeat kinase 2 (LRRK2) and DJ-1, are localized to mitochondria and involved in the regulation of mitochondrial dynamics in the same or parallel pathways[5-12]. Therefore, an altered balance in mitochondrial fission and fusion is likely a common mechanism leading to impaired mitochondrial quality control and mitochondrial dysfunction critical to PD pathogenesis[13].

Recently, vacuolar protein sorting 35 *(VPS35)* was identified as the third gene associated with autosomal-dominant PD[14-16] after *SNCA* and *LRRK2*. D620N is a mutational hotspot while R524W is a rare, less potent pathogenic variant[14-18]. As a key component of the retromer complex, VPS35 is important for endosome-to-Golgi and endosome-to-plasma membrane retrieval of membrane proteins[19,20]. Recent progress has extended the role of VPS35 in the formation of mitochondria-derived vesicles (MDVs)[21], which shuttles cargo from mitochondria to peroxisome or lysosome[22,23], suggesting mitochondria might be a possible action site for VPS35. Therefore, we explored the potential involvement of VPS35 in the regulation of mitochondrial dynamics and function. During fission, DLP1 is recruited to mitochondrial outer-membrane and forms a large ring-like complex to exert fission activity[24]. Our present study offers new insights into cellular mechanism underlying mitochondrial DLP1 complex turnover and pathogenic mechanism of VPS35 mutations in PD.

Results

VPS35 mutations cause mitochondrial fragmentation *in vitro*

Rat primary cortical neurons were transfected with mitoDsRed2 and VPS35 constructs and imaged for mitochondrial morphology. Vector-control neurons demonstrated tubular mitochondrial morphology with an average aspect ratio of 2.4 ± 0.2 (Fig. 1a-c). In contrast, neurons overexpressing wild-type (WT) VPS35 showed marked decrease in mitochondrial length (Supplementary Fig. 1a) and the average aspect ratio decreased to 1.87 ± 0.15 (Fig. 1a-c), suggestive of mitochondrial fragmentation. Mitochondria were similarly fragmented in neurons overexpressing R524W mutant which became more severe in neurons

Europe PMC Funders Author Manuscripts

overexpressing D620N mutant. Neurite mitochondrial index, an index for mitochondrial density, was also significantly reduced in neurons overexpressing WT or mutant VPS35 ($P < 0.05$, Supplementary Fig. S1b). We measured mitochondrial fission and fusion events by real-time imaging and found that the ratio of fission over fission-plus-fusion events was significantly increased in neurons overexpressing WT or mutant VPS35 ($P < 0.05$, Fig. 1d). Compared to vector-control neurons, WT or R524W VPS35 caused significant neuronal loss, which was more profound in D620N-overexpressing cells ($P < 0.05$, Fig. 1e).

We further determined whether VPS35 knockdown would induce an effect opposite to VPS35 overexpression. VPS35 expression was knocked down by two different VPS35 miR-based RNAi constructs, both of which significantly increased mitochondrial length and aspect ratio and decreased the ratio of fission over fission-plus-fusion events ($P < 0.05$, Supplementary Fig. 1). Interestingly, when neurons were treated with RNAi specifically suppressing VPS26, another subunit of the retromer complex[25], mitochondrial aspect ratio was similarly increased (Supplementary Fig. 2a,b). VPS26 knockdown did not induce further increase of aspect ratio in cells with concurrent VPS35 knockdown. More importantly, VPS35 overexpression-induced mitochondrial fragmentation could be abolished by concurrent VPS26 knockdown (Supplementary Fig. 2c,d), suggesting that VPS35 and VPS26 act through the same pathway.

Mitochondrial dynamics were also examined in stable lines of M17 human dopaminergic neuroblastoma cells (Supplementary Fig. 3). Consistent with our observations in primary neurons, mitochondrial aspect ratio decreased in M17 cells overexpressing WT (WT VPS35 M17 cells) or R524W VPS35 (R524W M17 cells), which was exacerbated in M17 cells overexpressing D620N VPS35 (D620N M17 cells). Mitochondria became elongated in M17 cells with suppressed VPS35 expression (VPS35 KD M17 cells) (Supplementary Fig. 4).

We further analyzed mitochondrial morphology in fibroblasts derived from PD subject bearing the VPS35 D620N mutation (D620N fibroblasts) and normal human fibroblasts (NHFs) from age-matched control subjects (Fig. 1f-i). Confocal analysis revealed an interconnected mitochondrial network in NHFs, which became significantly fragmented in D620N fibroblasts (Fig. 1f,g). Treatment with mitochondrial fission inhibitor-1 (e.g., mdivi-1)[26] restored mitochondrial length in D620N fibroblasts (Fig. 1f,g). Electron microscopy (EM) also demonstrated significantly fragmented mitochondria in D620N fibroblasts compared with NHFs (Fig. 1h,i).

VPS35 mutations cause mitochondrial fragmentation *in vivo*

To determine the effect of VPS35 mutants *in vivo*, we stereotactically injected mice with lentivirus co-expressing VPS35 (WT or mutants) and mitoDsRed2 unilaterally into the substantia nigra of 2-3 months old wild-type FVB or C57BL6 mice (Schematic in Fig. 2a) and imaged three weeks later. In both backgrounds, neurons expressing WT or R524W VPS35 exhibited fragmented mitochondria which became more profound in neurons expressing D620N mutant, distinct from the normal tubular shape in vector-control neurons from mice injected with mitoDsRed2 and empty-vector (Fig. 2b,c and Supplementary Fig. 5a,b). There was a trend towards more severe mitochondrial fragmentation in the TH–positive neurons than in the TH–negative neurons in mice injected with WT or R524W

VPS35 which became significant in mice injected with D620N VPS35 ($P < 0.05$, Fig. 2b,c). Significant and comparable levels of neuronal loss, both in TH–positive and TH–negative neurons, was observed in the mice injected with WT or R524W VPS35 (Fig. 2d-e and Supplementary Fig. 5c). The loss of TH–positive neurons, correlated with enhanced mitochondrial fragmentation (not shown), became more profound in mice injected with D620N VPS35. To determine the critical role of VPS35-induced mitochondrial fission *in vivo*, we treated VPS35-injected mice with mdivi-1. As expected, mdivi-1 blocked VPS35-induced mitochondrial fragmentation in both TH–positive (Fig. 2f,g) and TH–negative neurons (not shown) in the substantia nigra. More importantly, mdivi-1 also prevented VPS35-induced neuronal loss *in vivo* (Fig. 2h).

VPS35 mutations cause mitochondrial dysfunction

We assessed the effect of VPS35 mutations on mitochondrial function, as well as on neuronal morphology and viability. Compared with vector-control M17 cells, we observed substantial mitochondrial dysfunction in WT VPS35 and R524W M17 cells which was worsened in D620N M17 cells, as evidenced by significantly increased mitochondrial reactive oxygen species generation (ROS, not shown) and decreased ATP levels and mitochondrial membrane potential (MMP) ($P < 0.05$, Fig. 3a,b). Measurement of oxygen consumption rates using the Seahorse XF24 analyzer[27,28] revealed impaired bioenergetics in these VPS35-expressing M17 cells as evidenced by significantly reduced respiratory control ratio, spare respiratory capacity and the coupling efficiency (Supplementary Fig. 6). Similar mitochondrial dysfunction (i.e., increased mitochondrial ROS and decreased MMP) induced by VPS35 expression was also found in primary cortical neurons (not shown). Importantly, D620N fibroblasts also demonstrated mitochondrial dysfunction (Fig. 3c,d) and impaired bioenergetics (Supplementary Fig. 7) compared to NHFs. Loss of dendritic spines and PSD95-positive boutons was apparent in primary neurons expressing WT or mutant VPS35 (Fig. 3e-g).

To determine whether excessive fission underlies VPS35-induced mitochondrial and neuronal deficits, we inhibited mitochondrial fission by overexpressing the dominant-negative DLP1^{K38A} mutant or by treating with mdivi-1 which successfully blocked mitochondrial fragmentation (Fig. 3h-j). Mdivi-1 did not affect DLP1 expression and phosphorylation (Supplementary Fig. 8). The inhibition of mitochondrial fragmentation rescued VPS35-induced mitochondrial dysfunction in both neuronal cells overexpressing VPS35 (Fig. 3a,b) and D620N fibroblasts (Fig. 3c,d and Supplementary Fig. 7). Neuronal deficits (i.e., loss of spines and PSD95 immunoreactivity) (Fig. 3e-g) were also rescued.

VPS35 regulates mitochondrial DLP1 complex turnover

Western blot demonstrated that total DLP1 levels slightly increased in VPS35-overexpressing M17 cells and decreased in VPS35 KD M17 cells (Supplementary Fig. 9). Real-time PCR confirmed a significant increase in DLP1 mRNA levels in VPS35-overexpressing M17 cells (not shown). No significant change in other fission and fusion proteins was noted.

Compared with vector-control lines, mitochondrial DLP1 was significantly increased in WT VPS35 or R524W M17 cells which became more profound in D620N M17 cells, but significantly reduced in VPS35 KD M17 cells ($P < 0.05$, Fig. 4a,b), suggesting that VPS35 facilitates mitochondrial translocation of DLP1 which is enhanced by PD-associated mutations. To corroborate this finding, we imaged mitochondrial DLP1 in fixed M17 cells after DLP1 immunostaining. Surprisingly, the mitochondrial DLP1 puncta density, along with their average size, was significantly decreased in VPS35-overexpressing M17 cells, but significantly increased in VPS35 KD M17 cells ($P < 0.05$, Fig. 4c,d). Given that mitochondrial DLP1 assembles into large complexes and DLP1 puncta on mitochondria likely represents mitochondrial DLP1 complex[29], this finding implicates that VPS35 may regulate the clearance of mitochondrial DLP1 complexes and facilitate the recruitment of fission-competent forms of DLP1.

To test this possibility, we expressed GFP-tagged DLP1 (GFP-DLP1) in M17 cells and used fluorescent recovery after photobleaching (FRAP) technique to measure the lifetime of mitochondrial GFP-DLP1 puncta by real-time imaging. VPS35 overexpression significantly shortened while VPS35 knockdown significantly extended the lifetime ($P < 0.05$, Fig. 4e). This is unlikely due to the difference in diffusion-limited kinetics because the fluorescence recovery of mitochondrial GFP-DLP1 was not dependent on the size of the bleached area and all stable cells lines had similar GFP-DLP1 recovery in cytosolic areas without mitochondria (not shown). To determine the levels of mitochondrial DLP1 complexes, large mitochondrial protein complexes were precipitated by ultracentrifugation (270K g) of mitochondrial fractions prepared from cells exposed to reversible crosslinking agent (i.e., DTME) and analyzed by SDS-PAGE. DLP1 levels were significantly decreased in the precipitates from WT VPS35 M17 cells but significantly increased in that of VPS35 KD M17 cells (Fig. 4f). Importantly, DLP1 levels were also significantly decreased in ultracentrifugation precipitates from D620N fibroblasts compared to that of NHFs ($P < 0.05$, Fig. 4g). The use of irreversible crosslinking agent (i.e., DSS) allows direct detection of oligomeric DLP1 complexes and monomeric DLP1[29-32]. Indeed, western blot of mitochondrial fractions from DSS–exposed cells demonstrated that levels of oligomeric DLP1 complexes were significantly decreased in VPS35-overexpressing cells but significantly increased in VPS35 KD M17 cells (Fig. 4h-i). In contrast, the monomeric mitochondrial DLP1 was significantly increased in VPS35-overexpressing cells but decreased in VPS35 KD cells (Fig. 4h,i). Knockdown of VPS26 increased mitochondrial DLP1 puncta and DLP1 complex levels but did not cause a further increase in cells with concurrent VPS35 knockdown (Supplementary Fig. 10a,b). More importantly, the effect of VPS35 overexpression on mitochondrial DLP1 complexes could be reversed by VPS26 knockdown (Supplementary Fig. 10c).

VPS35–DLP1 interaction is key to mitochondrial DLP1 turnover

To determine the biochemical basis of the regulatory role of VPS35 in mitochondrial dynamics, we investigated whether VPS35 interacts with DLP1. M17 cells transfected with mitoDsRed2 and immunostained with antibodies against DLP1 and VPS35 were imaged and 3D reconstructed images demonstrated the colocalization of DLP1 puncta and VPS35 on mitochondria (Fig. 5a). We found a strong interaction between VPS35 and DLP1 by yeast

two-hybrid analysis (Fig. 5b). In M17 cells, endogenous VPS35 could be co-immunoprecipitated (co-IP) by DLP1 antibody and *vice versa* (Fig. 5c,d). We confirmed the presence of endogenous VPS35 in pure mitochondrial fractions (Fig. 5e)[21]. Indeed, endogenous DLP1 co-IP with VPS35 in mitochondrial fractions (Fig. 5f). Significantly more DLP1 were pulled down by VPS35 antibody in D620N M17 cells compared to WT VPS35 M17 cells which suggested enhanced interaction between DLP1 and D620N mutant (Fig. 5f). Indeed, increased VPS35–DLP1 interaction was confirmed in the D620N fibroblasts compared to that in NHFs (Fig. 5g). Increased VPS35–DLP1 interaction was also found in H_2O_2– or paraquat–treated M17 cells, which was inhibited by concurrent treatment with the antioxidant N-acetylcysteine (Supplementary Fig. 11), suggesting that oxidative modification may enhance VPS35–DLP1 interaction. Increased oxidative stress is a prominent feature of PD[2] and increased VPS35–DLP1 interactions were found in post-mortem brain samples of sporadic PD subjects (Fig. 5h).

D620N enhanced VPS35–DLP1 interaction (Fig. 5f,g). Not surprisingly, artificial mutations at this site differentially impacted VPS35–DLP1 interaction: D620E and D620I decreased, D620A and D620R did not affect, and D620Y increased such interaction (Fig. 5i). These mutants had differential rescuing effects on mitochondrial DLP1 complex accumulation in VPS35 KD M17 cells: overexpression of WT, D620A or D620R significantly reduced mitochondrial DLP1 complex levels in the 270K g precipitates while overexpression of D620N or D620Y caused further reductions ($P < 0.05$). Overexpression of D620E or D620I failed to do so (Fig. 5j). Consistently, these mutants also had differential rescuing effects on elongated mitochondrial morphology in VPS35 KD M17 cells: their overexpression could enhance fission to restore the normal filamentous mitochondrial morphology (WT, D620A, D620R) or make it even shorter (D620N, D620Y), or failed to rescue elongated mitochondrial morphology (D620E, D620I) in VPS35 KD M17 cells (Supplementary Fig. 12a,b), suggesting fission deficits of the latter two mutants. In a control experiment, we found that reducing VPS35 reduced retromer function as evidenced by reduced fatty-acid translocator (FAT)/CD36 recycling in VPS35 KD cells [33], and each of these artificial mutations could restore FAT/CD36 recycling to a level comparable to WT VPS35 (Supplementary Fig. 12c), which demonstrated that none of these mutations impaired the retromer function. Collectively, these data strongly supported that VPS35–DLP1 interaction is essential for mitochondrial DLP1 complex turnover required for efficient mitochondrial fission.

MDV mediates VPS35-dependent mitochondrial DLP1 turnover

Retromer is involved in MDV formation and MDVs can transport mitochondrial proteins to lysosomes[22,34]. We investigated whether DLP1 localized to MDVs. MDVs contain mitochondrial outer-membrane proteins such as TOM20 but not matrix proteins such as COX-IV and mitoDsRed2[21]. To reconstitute MDVs *in vitro*, we used a cell-free budding assay[35]. Western blot demonstrated the presence of TOM20 and absence of COX-IV in the post-mitochondria supernatant treated with trypsin (Fig. 6a), confirming the successful MDVs reconstitution *in vitro*. As expected, TOM20 signal was enhanced by cytosol and abolished by N-ethymaleimide, a cell-free membrane transport inhibitor (Fig. 6a). DLP1 behaved similarly to TOM20 (Fig. 6a), suggesting that DLP1 is a cargo of MDVs. The

enrichment of DLP1 in trypsin-treated supernatant was time-dependent which was more significantly stimulated by the cytosol from VPS35-overexpressing cells but less significantly stimulated by that from VPS35 KD M17 cells compared with that from vector-control M17 cells ($P < 0.05$, Fig. 6b,c).

60-100 nm vesicular structures attached to mitochondrion, with either double– or single–membrane, consistent with previously described MDVs[36], were readily observed in purified mitochondria by EM (Fig. 6d). Immuno-EM with the highly specific DLP1 antibody (Supplementary Fig. 13) revealed the presence of DLP1-positive immunogold particles in these MDVs (Fig. 6e). This is corroborated by confocal imaging in which DLP1 puncta co-localized with TOM20-positive and mitoDsRed2-negative MDVs in M17 cells (Fig. 6f). In fact, the colocalization of DLP1 and MDVs was significantly increased in VPS35-overexpressing M17 cells but decreased in VPS35 KD M17 cells (Fig. 6g,h), suggesting that VPS35 mediates the MDV-dependent transport of DLP1.

3D reconstructed images showed the presence of DLP1 puncta-associated MDVs in lysosome (Fig. 6i) which was reduced by VPS35 knockdown but increased by overexpression of WT or D620N VPS35 (Fig. 6j). DLP1 puncta-associated MDVs in lysosome are inversely correlated with the density of mitochondrial DLP1 puncta (not shown). Indeed, inhibition of lysosomal degradation by bafilomycin A1 leads to increased accumulation of DLP1 puncta-associated MDVs in lysosome (Fig. 6j), which thus confirms the final fate of degradation of the DLP1 complexes trafficked to lysosome through MDVs. We found no difference in DLP1 levels in peroxisomes between cells with VPS35 overexpression or knockdown (Supplementary Fig. 14), implicating that VPS35-dependent DLP1-MDVs do not traffic to peroxisomes.

Discussion

The most important and novel finding in this study was that PD-associated VPS35 mutation caused extensive mitochondrial fragmentation and functional deficits as well as neuronal loss both *in vitro* and in the substantia nigra of mouse brain *in vivo* which can be rescued by inhibition of excessive mitochondrial fission, suggesting that VPS35 mutation likely caused neurodegeneration through damaging effect on mitochondrial dynamics and dysfunction. The effect of PD-associated VPS35 mutation on mitochondrial dynamics and dysfunction is likely a specific effect of the mutation independent of potential overexpression artifacts because 1) in fibroblasts from PD subject bearing VPS35 mutation, mitochondria became fragmented and functionally impaired; 2) elongated mitochondria were found in VPS35 KD M17 cells which can be restored to normal filamentous shape by re-expression of WT VPS35, but which became fragmented by similar levels of VPS35 D620N expression; 3) VPS35–DLP1 interaction was found in normal M17 and NHFs which was enhanced in fibroblasts from PD subject with D620N mutation.

Mechanistically, we described a novel concept for the biology of mitochondrial fission by revealing the involvement of VPS35 and retromer in the recycling of mitochondrial DLP1 complexes and the regulation of mitochondrial fission (Supplementary Fig. 15). DLP1 complexes on mitochondrial outer-membrane remains with daughter mitochondrion after

fission[37] which likely become inhibitory for subsequent fission either due to the occupancy of fission sites, sequestration of DLP1 recruiting factors, or spatial blockage[29-32,38,39]. In this study, we demonstrated that retromer, through VPS35–DLP1 interaction, mediates the removal of these DLP1 complexes from mitochondria and transports them to lysosomes for degradation via the formation and trafficking of MDVs, thus effectively alleviating the inhibitory effects, which is likely a critical process required for efficient mitochondrial fission. PD-associated VPS35 mutation caused increased VPS35–DLP1 interaction, and enhanced retromer-dependent turnover of mitochondrial DLP1 complex through MDV-mediated trafficking and tipped the mitochondrial dynamics balance towards excessive fission, which leads to mitochondrial dysfunction and neuronal loss[40]. We further demonstrated increased oxidative stress enhanced VPS35–DLP1 interaction which likely underlies similarly increased VPS35–DLP1 interaction in the brains of sporadic PD subjects. These data support a more general role of the dysregulation of VPS35-mediated mitochondrial DLP1 complex turnover in causing abnormal mitochondrial dynamics and mitochondrial dysfunction critical to PD pathogenesis.

Various PD-associated proteins are involved in the regulation of mitochondrial dynamics. PINK1/Parkin regulates the ubiquitination and degradation of Mfn2 and DLP1 while LRRK2 increased DLP1 recruitment to mitochondria[5,8,9]. Our current study revealed a novel cellular mechanism for the regulation of mitochondrial fission at the level of mitochondrial DLP1 complex turnover which was enhanced by PD-associated VPS35 mutation. Nevertheless, our study does not exclude the possibility that other cellular function may be negatively impacted by VPS35 mutations. Recent studies revealed D620N mutation also leads to a defect in the WASH complex binding and perturbation in endosome-to-Golgi transport and autophagosome biogenesis[41-43].

Materials and Methods

Cell culture and transfection

Human neuroblastoma M17 cells were grown in Opti-MEM medium (Invitrogen), supplemented with 5% or 10% (v/v) fetal bovine serum and 1% penicillin–streptomycin (P/S), in 5% CO_2 in a humid incubator at 37 °C. They were tested free of mycoplasma contamination. Regular culture medium containing 300 μg/ml Geneticin (Invitrogen) or 20 μg/ml Blasticidin (Invitrogen) was used for stable cell line selection. Three independent clones of M17 cells stably knocking down or overexpressing wild type (WT) or mutant VPS35 (R524W and D620N) were established. Primary neurons from embryonic day 18 (E18) rat cortex were isolated from rats (Harlan). Only female pregnant rats (9–10 weeks old) were used for primary neuron isolation every other week on a continual basis under protocol approved by the Institutional Animal Care and Use Committee (IACUC) at Case Western Reserve University. Briefly, pregnant female rat at E18 was anesthetized and then the embryos were dissected out in dissection buffer (HBSS, 20 mM HEPES, 20 mM Glucose). The head of embryo was removed and placed in 1.5 ml tubes containing Hibernate E (BrainBits) with 2% B27 (Invitrogen). Under a dissecting microscope, the skull was removed and the meninges carefully stripped away with fine forceps in dissection buffer. The cortex of both hemispheres was dissected out after removing the hippocampus. The

cortical tissue was placed in digestion solution (0.25% trypsin, 20 mM Glucose, 20 mM HEPES, DNAse 50 unit/ml) for 15 min at room temperature. The trypsin was stopped by adding 15% FBS in OPTI-MEM. The tissue was dissociated using a one ml pipette by gently triturating on the side of the tube 15 times until no big chunks of tissue remain. Centrifuge at 200 × g for 2-3 min and resuspend the cell pellet into day zero culture media (neurobasal medium, 2% B27, 1% GlutaMAX, 1% P/S (Invitrogen). Primary neurons were seeded at 400,000 cells per coverslips (15 mm) coated with poly-L-lysine. Change media the next day to culture media without P/S. All cultures were kept at 37 °C in a humidified 5% CO_2-containing atmosphere. More than 90% of the cells were neurons after they were cultured for 7–17 d of culture day *in vitro* (DIV), which was verified by positive staining for the neuronal specific markers microtubule-associated protein-2 (MAP2, dendritic marker) and Tau-1 (axonal marker). At DIV 7–12, neurons were transfected using Neurofect (Genlantis) according to the manufacturer's protocol. M17 cells are transfected by Lipofectamine 2000 (Invitrogen) and transfection efficiency is almost 80% as confirmed by immunofluorescence.

Expression vectors, antibodies, chemicals and measurement

MitoDsRed2 construct (Clontech), mito-TagBFP2 construct (Evrogen), green fluorescent protein (GFP)-tagged wild-type DLP1 (DLP1wt), dominant-negative mutant $DLP1^{K38A}$ (gifts from Dr. Yisang Yoon, University of Rochester, Rochester, NY). The expression plasmids for flag-tagged VPS35 were constructed based on the pCMV-3Flag-1a vector (Agilent). The micro-RNA (miR) RNA interference (RNAi) vector was generated via the pcDNA 6.2-GW/EmGFP-miR construct (Invitrogen). The miR RNAi sequences targeting different mRNA regions of exon 5 on the open reading frame region of human/rat/mouse VPS35 were: TCGCTTCACACTGCCACCTTT (#1) and TTCACACTGCCACCTTTGGTA (#2). The pre-designed siRNA targeting to VPS26 was: GCCUUACCUGGAGAACUCAtt (Invitrogen). Primary antibodies used include mouse anti-DLP1 (BD Biosciences, Catalog Number 611112, 1: 5,000 dilution), mouse anti-Mfn1 (Santa cruz, Catalog Number sc-50330, 1: 2,000 dilution), anti-Mfn2 (Santa cruz, Catalog Number sc-100560, 1: 2,000 dilution) mouse anti-NeuN (Millipore, Catalog Number MAB377, 1: 300 dilution), mouse anti- β -actin (Chemicon, Catalog Number MAB1501, 1: 10,000 dilution), rabbit anti- β -III-tubulin (Cell Signaling, Catalog Number 2125, 1: 300 dilution), rabbit anti-DLP1 (Cell Signaling, Catalog Number 8570, 1: 50 dilution), mouse anti-α-tubulin (Cell Signaling, Catalog Number 3873, 1: 300 dilution), mouse anti-Tom20 (BD Biosciences, Catalog Number 612278, 1: 2,000 dilution), mouse OXPHOS cocktail (Abcam, Catalog Number ab110411, 1: 2,000 dilution), mouse anti-COX IV (Cell Signaling, Catalog Number 4850, 1: 5,000 dilution), mouse anti-Flag (Cell Signaling, Catalog Number 8146, 1: 10,000 dilution), rabbit anti-VPS35 (Epitomics, Catalog Number 7514-1, 1: 2,000 dilution), rabbit anti-VPS26 (Abcam, Catalog Number ab23892, 1: 2,000 dilution), rabbit anti-Tyrosine hydroxylase (Abcam, Catalog Number# Ab112, 1: 300 dilution), rabbit anti-PEX19 (Pierce, Catalog Number PA5-22129, 1: 300 dilution). DLP1 inhibitor mdivi-1 was obtained from Enzo and H_2O_2, paraquat dichloride, N-acetylcysteine, bafilomycin A1 was obtained from Sigma. H_2O_2 (Sigma), dithiobismaleimidoethane (DTME) (Pierce) were also obtained. Cell death in M17 cells was measured by Cytotoxicity Detection Kit (LDH; Roche). ATP levels were measured by the ATP Colorimetric-Fluorometric Assay Kit (Biovision). The ROS level

and mitochondrial membrane potential was measured as described before[4]. Neuronal viability propidium iodide assay in cultured primary neurons was performed as described previously[44].

Lentivirus production, stereotaxic injection and cyrosection

Mice surgery and procedures were performed according to the NIH guidelines and were approved by the Institutional Animal Care and Use Committee (IACUC) at Case Western Reserve University. Minimal number of mice was used (n = 3–4 per group). 2-3 months old FVB (n = 3 per group) or C57BL/6J mice (n = 4 per group), both male and female, were randomly assigned to receiving different injections. Lentivirus expression plasmids were constructed by inserting VPS35-p2a-mitoDsRed2 fragment into Plvx-Puro from Clontech. Lenti-X 293T cells (Clontech) were transfected with the expression plasmids and two helper plasmids (addgene): Δ8.2 and vesicular stomatitis virus G protein at 6 μg, 4.5 μg, and 1.5 μg of DNA per 10 cm plate using PerFectin (Genlantis). 48 hours after transfection, the supernatants of eight plates were pooled, centrifuged at 780 g for 30 min, filtered at a 0.45 μm pore size. The supernatants were laid on the top of 20% sucrose and centrifuged in a Beckman SW-28 rotor at 110,000 g for 2 h, and the pellet was resuspended in 100 μl of PBS. Mice were anesthetized using avertin at 2.5% (v/v) and placed in a stereotactic frame. A small incision was made to expose the skull surface and to visualize bregma. Holes were drilled in the skull overlying the VTA (AP - 3.3, ML −0.8) and 10 μl microsyringe (Hamilton) filled with virus. The needle was lowered down 4.6 mm from the bregma, 1 μl virus (109 viral particles/ml) was injected within 5 min and the needle left in place 5 min before slowly withdrawing it. The skin was sutured and mice were allowed to recover. Three weeks after virus injection, mice were deeply anesthetized with avertin and transcardially perfused with cold PBS. The brain was dissected out and immersion-fixed in paraformaldehyde for 24 h and then in 30% sucrose for 24 h. After cryoprotection, the brain was frozen in −80 °C and coronal sections were cut in 20 μm. Three serial sections around the virus injection site which cover the substantia nigra region were immunostained with anti-TH antibody and anti-NeuN antibody. The number of TH-positive and TH-negative neurons were identified by ImageJ software and the percentage of neuronal loss was calculated and averaged by comparing the neuronal number between virus injected side and non-injected side and normalized to the mice injected with vector. The outcomes were independently assessed by an investigator without knowledge of treatments.

Western blot and immunoprecipitation

Cells were lysed with 1 × Cell Lysis Buffer (Cell Signaling) or RIPA buffer, plus 1 mM phenylmethylsulfonyl fluoride (Sigma) and Protease Inhibitor Cocktail (Sigma). Equal amounts of total protein extract (5 or 20 μg) were resolved by sodium dodecyl sulfate polyacrylamide gel electrophoresis and transferred to Immobilon-P (Millipore). Following blocking with 10% nonfat dry milk, primary and secondary antibodies were applied, and the blots were developed with Immobilon western Chemiluminescent HRP Substrate (Millipore). Immunoprecipitation was performed with antibodies against DLP1, Flag or VPS35 in RIPA buffer using Dynabeads Protein G-IP Kit (Invitrogen) and analyzed by western blot.

Human brain samples

Frozen samples of human brain substantia nigras from PD cases (n = 5, ages = 75–88 years, postmortem interval = 5.5–18.8 h) and gender- and age-matched controls (n = 5, ages = 77–86 years, postmortem interval = 3–19 h) were obtained from the Harvard Brain Tissue Resource Center, NIH Neurobiobank and Case Western Reserve Brain Bank under protocols approved by Institutional Review Board for Human Investigation at Case Western Reserve University. Tissues were homogenized in RIPA buffer, centrifuged at 18,000 g for 15 min at 4 °C. Equal amounts of protein extracts were used for immunoprecipitation by immobilized anti-DLP1 antibody.

Mitochondria isolation

Crude and purified mitochondria was isolated as described[5] with modification. Briefly, cells were trypsinized, washed in PBS and resuspended in a minimal volume of IB-1 solution (IB-1: 225 mM Mannitol, 75 mM sucrose, 0.1 mM EGTA, 20 mM Hepes pH=7.4). The cells were homogenized until ~80% of cell breakage and then centrifuged at 600 g for 5 mins to remove nuclear contaminants and unbroken cells. The supernatant was once again centrifuged at 600 g for 5 mins, followed by a centrifugation at 7,000 g for 10 mins to isolate mitochondria and the supernatant was collected as the cytosolic fraction. The mitochondrial pellet was washed in 20 ml IB-2 solution (225 mM Mannitol, 75 mM sucrose, 20mM Hepes pH=7.4), centrifuged at 7,000 g for 10 mins, resuspended in 20 ml IB-2 solution, centrifuged at 10,000 g for 10 min and finally resuspended in 2 ml MRB buffer (250 mM Mannitol, 5 mM Hepes, 0.5 mM EGTA, pH 7.4) to make crude mitochondria. The crude mitochondrial fraction was overlaid on top of 8 ml Percoll medium (225 mM mannitol, 25 mM Hepes pH 7.4, 1 mM EGTA and 30% Percoll (vol/vol)). MRB was added on top of the mitochondrial layer, followed by centrifugation at 95,000 g in a SW40 rotor for 30 minutes at 4 degrees. The purified mitochondrial fraction was collected and resuspended in 20 ml MRB buffer and centrifuged 10 mins at 6,300 g. The pellet was resuspended in 1 ml MRB buffer, centrifugatd at 6,300 g in an Eppendorf microcentifuge for 2 minutes. Isolated mitochondria were lysed with Cell Lysis Buffer (Cell Signaling) or RIPA buffer, and then underwent direct western blot analysis or immunoprecipitation.

Live cell crosslinking

M17 cells were seeded into the six well plate for 24 hrs. After a wash with PBS, cells were incubated with HBSS containing 0.5 mM dithiobismaleimidoethane (DTME, from freshly prepared stocks in DMSO) for 5 mins or Opti-MEM culture medium containing 0.25 mM disuccinimidyl suberate (DSS, from freshly prepared stocks in DMSO) for 30 mins at 37 °C. The HBSS/DTME or Opti-MEM/DSS was removed and mitochondria fraction was isolated. For DTME crosslinking, mitochondria were lysed in buffer containing 60 mM Tris pH 6.8 and 0.2% SDS. Insoluble debris was removed by centrifugation (10 min at 14,000 g) and cleared lysates were layered onto 1 ml of a 300 mM sucrose cushion and subjected to ultracentrifugation (30 min at 300,000 g). Pellets were dissolved in SDS sample buffer containing 5% β-mercaptoethanol to cleave the crosslinker and analyzed by SDS-PAGE. For DSS crosslinking, mitochondria were lysed in Cell Lysis Buffer and directly subjected to SDS-PAGE.

Immunofluorescence, fluorescence recovery after photobleaching (FRAP) and time-lapse imaging

For immunofluorescence, neuronal cells cultured on four or eight well chamber slides were fixed and stained. All fluorescence images were captured at room temperature with a Zeiss LSM 510 inverted laser-scanning confocal fluorescence microscope (controlled through Zeiss LSM 510 confocal software, Zeiss) equipped with an Alpha-Plan Fluor 100 × NA 1.45 oil objective (working distance: 0.11 mm; Zeiss). Confocal images of far-red fluorescence were collected using 633 nm excitation light from a HeNe laser and a 650 nm long-pass filter; images of red fluorescence were collected using 543 nm excitation light from an argon laser and a 560 nm long-pass filter; and green fluorescence images were collected using 488 nm excitation light from an argon laser and a 500–550 nm bandpass barrier filter. For fluorescence recovery after photobleaching (FRAP), M17 cells were seeded on glass bottom microwell dishes (MaTek) for 24 hours and then transfected with mitoDsRed2 and GFP-DLP1 plasmids. Using the 488 nm laser line of a Zeiss LSM 510 confocal microscope, GFP-DLP1 fluorescence of a selected region was bleached and fluorescence recovery was tracked by capturing images every 5 s for 5 min. Image stacks were analyzed, and recovery curves normalized to pre-bleach intensity and corrected for acquisition bleach by ImageJ. Time-lapse tracking of DLP1 and VPS35 was imaged by spinning disk confocal (PerkinElmer) using 63 × objective, and frames were captured every three seconds for 10 min in a well-equipped environmental chamber with controlled CO_2 content, humidity and temperature and imaged at 37 °C.

Image analysis

Image analysis was performed with open-source image-analysis programs WCIF ImageJ (developed by W. Rasband). Mitochondria morphology was quantified as previously described[44]. Taken briefly, raw images were background corrected, linearly contrast optimized, applied with a 7 × 7 “top hat” filter, subjected to a 3 × 3 median filter and then thresholded to generate binary images. Most mitochondria were well separated in binary images and large clusters of mitochondria were excluded automatically. All binary images were analyzed by ImageJ to provide information of mitochondria aspect ratio (ratio between major and minor axes of an ellipse equivalent to the mitochondrion as an index for mitochondrial morphology). The researchers counting mitochondria abnormalities or cell death were all blinded to the identity of the experiment.

Yeast Two Hybrid

Yeast two hybrid experiments were performed using the Matchmaker GAL4 Two-Hybrid (Clontech) System 3 with vectors pGBKT7 and pGADT7 containing the binding domain and activation domain respectively. Yeast strain AH109 (Clontech) was transformed with empty pGBKT7 and pGADT7 vectors or pGBKT7 and pGADT7 vectors encoding DLP1 or VPS35 using Yeast Transformation Kit (Clontech). After transformation, yeast cells were plated on SD/-Leu/-Trp plates followed by streaked onto high-stringency plates (SD/-Leu/-Trp/-His/-Ade). β-Galactosidase activity in different yeast clones was measured by Yeast beta-Galactosidase Assay Kit (Piercenet) following Manufacturer’s instructions.

Human Fibroblasts

Primary human fibroblast from a PD patient bearing VPS-35 D620N mutation was generated and characterized as previously published[41]: Briefly, from the forearm of a healthy donor patient and a Parkinson's disease patient genotyped to harbor the VPS35(D620N) mutation, two 2 mm^2 skin biopsies were taken. These were each placed into a sterile sample tube (Sterilin, UK) along with 10 ml of fibroblast media prior to transportation to the lab on wet ice (total time < 30 mins). The epidermis and any fat were removed (sterile scalpel and forceps) prior to cutting into 4 roughly equal pieces, which were placed into a 4 well plate (Nunc) pre-coated with CELLstart™ ((1:200 in PBS(+/+)), Sigma D8662) in 200 μl of fibroblast media (DMEM (Sigma, D6546) supplemented with 10% heat inactivated foetal bovine serum, (Invitrogen, 10500), 1% Glutamax™ (Invitrogen, 35050), 1% NEAA (Invitrogen, 11140), 1% penicillin-streptomycin (Sigma, P4458)). Cultures were left for up to two weeks to allow cell attachment to the matrix and dermal fibroblasts proliferation. At 80% confluency cells were enzymatically passaged using TrypLE Express (Gibco, 12604) and passaged at a ratio of 1:3 until cryopreserved.

Primary human fibroblasts from four gender- and age-matched normal subjects (Normal Human Fibroblasts, NHFs) were obtained from Coriell Institute for Medical Research. Primary fibroblasts were grown in minimum essential medium (Invitrogen) containing non-essential amino acids and 2 mM glutamine, supplemented with 10% or 15% (v/v) fetal bovine serum, in 5% CO_2 in a humid incubator at 37 °C. Fibroblasts cells were transfected with Effectene Transfection Reagent (Qiagen) according to manufacturer's protocol and imaged as we previously reported[45].

In vitro reconstitution of MDVs

Mitochondrial budding assay was performed as previously reported[35] with minor modification. Briefly, isolated mitochondria from mouse liver were washed three times and then resuspended in the mitochondria resuspending buffer (250 mM Mannitol, 5 mM hepes, 0.5 mM EGTA, pH 7.4). M17 cells were seeded in the 10 cm dish and cells were harvested after trypsin. Cells were homogenized in IB-1 buffer (IB-1: 225 mM Manitol, 75 mM sucrose, 0.1 mM EGTA, 20 mM hepes, pH=7.4) and cytosol fraction were prepared by centrifuge at 180,000 g for 30 min. Cytosol fraction of each cell lines were aliquoted and stored in −80 °C. For budding assay, mitochondria (1 mg) were incubated with or without cell cytosol fraction (200 μg) at room temperature in a final 100 μl system with following reagents: 225 mM mannitol, 75 mM sucrose, 80 mM KCl, 0.1 mM EGTA, 20 mM Hepes, 1.6 mM $MgCl_2$, 1.6 mM ATP, 5 mM succinate, 2 mM K_2HPO_4, 0.3 mM phosphocreatine, 8.3 mg/ml creatine phosphokinase, pH 7.4). In control experiment, 10 mM N-ethylmaleimide (NEM, Sigma) was added to the reaction to inhibit the budding process. After reaction, mitochondria were removed by centrifugation at 10,000 g and supernatant fraction was further treated by 0.25% trypsin for 5 min at room temperature. Then samples were lysed by 10 × cell lysis buffer for western blot.

Transmission Electron Microscopy (TEM) and Immuno-electron microscopy (IEM)

TEM: Fibroblasts were seeded onto a sterilized Aclar Embedding Film (Electron Microscopy Sciences, PA), lining the wells in a 6-well cell culture cluster. After the cells had

Europe PMC Funders Author Manuscripts

reached ~80% of confluence, the Aclar sheets with their attached cells were immersed in fixative. The initial fixative was 0.25% glutaraldehyde in cacodylate buffer (pH 7.3). The specimen was postfixed in ferrocyanide-reduced 1% osmium tetroxide. The samples were processed as previously reported[46].

An aliquot of isolated mitochondrial suspension prepared from mouse liver was added to an equal volume of half half-strength Karnovsky's fixative and immediately spun down in a microfuge (4,000 g). The resultant pellet was transferred to fresh quarter-strength Karnovsky's fixative. After a rinse in buffer, the pellet was postfixed in ferrocyanide reduced osmium tetroxide, then rinsed in distilled water. The pellet was soaked overnight in acidified 0.25 % uranyl acetate, and embedded in Poly/Bed 812, then examined in a JEOL 1200EX electron microscope, Zeiss CEM 902 Electron microscope, and FEI Tecnai Spirit (T12) with a Gatan US4000 4k × 4k CCD.

IEM: Isolated mitochondria prepared from mouse liver were fixed in 4% w/v formaldehyde containing 0.1% w/v glutaraldehyde in 0.1 M HEPES buffer (Electron Microscopy Sciences, Hatfield, PA) at RT for 45 min, then dehydrated in ethanol and embedded in LR White resin (Polysciences, Inc., Warrington, PA). Immuno-gold labeling procedure was performed according to the method described by Fujioka et al[47]. Thin sections were blocked with PBS containing 1% w/v bovine serum albumin (BSA), 1% v/v normal goat serum and 0.01% v/v Tween 20 (PBGT). Grids were then incubated with mouse anti-DLP1 antibody at 1:8 dilution in PBGT for 12 h at 4°C. Negative controls included normal mouse serum and PBT replaced as the primary antibody. After washing, grids were incubated for 1 h in 10 nm gold-conjugated goat anti-mouse IgG (British BioCell International, Ted Pella, Inc., Redding, CA) diluted 1:30 in PBGT, rinsed with PBS, and fixed with glutaraldehyde to stabilize the gold particles[47]. Gold-labelled thin sections were stained first with 2% uranyl acetate in 50% methyl alcohol acidified uranyl acetate at 38 °C for 30 min, then with the triple lead stain of Sato as modified by Hanaichi et al[48], then examined in a JEOL 1200EX electron microscope, Zeiss CEM 902 Electron microscope, and FEI Tecnai Spirit (T12) with a Gatan US4000 4k × 4k CCD.

Seahorse XF24 mito-stress analysis

M17 neuroblastoma cells were cultured in Seahorse XF-24 (Seahorse Bioscience, Billerica, USA) plates which were coated with poly-D lysine (50 μg/ml). M17 cells were seeded at a density of 100,000 cells per well. For primary fibroblasts, cells were seeded at a density of 50,000 cells per well. Before assay, culture medium was changed to unbuffered DMEM (DMEM base medium supplemented with 25 mM glucose, 1 mM sodium pyruvate and 1 mM GlutaMAX) and cells were incubated at 37 °C in a non-CO_2 incubator for 45 min. The assay protocol consisted of repeated cycles of 3 min mixing, 2 min wait and 3 min measurement periods. Basal OCR was measured three times before drug exposure. Then oligomycin (1 μM), FCCP (0.5 μM for M17 cells and 2 μM for primary fibroblasts) and rotenone/antimycin A (0.5 μM) were injected sequentially into the media in each well. After injection of each drug, OCR measurements were made three times. After the assays, protein concentrations for each well were measured to confirm the similar cell number seeded.

FAT/CD36 receptor recycling assay

Receptor recycling assays were performed as previously described[33] with minor modification. VPS35 KD M17 cells were seeded in 4-well glass chamber slide at a density of 100,000 cells per well in 5% FBS of Opti-MEM. Cells were transfected with plasmids containing VPS35 artificial mutations for 72 hours. Culture medium was changed to Opti-MEM with 10% FBS for two hour at 37 °C, then cells were incubated in Opti-MEM (1% FBS) with antibody against FAT/CD36 (Santa Cruz) for one hour at 37 °C. Cells were acid washed with cold Opti-MEM (pH 2.0) and then were cultured in Opti-MEM with 10% FBS for another one hour at 37 °C. Then cells were incubated in Opti-MEM (1% FBS) with Alexa Fluor 568 conjugated anti-rabbit antibody for one hour at 37 °C. Cells were again acid washed with cold Opti-MEM at pH 2.0. Cells were then fixed with 4% paraformaldehyde for 15 min and were permeabilized with 0.5% Triton X-100 for 40 min. Positively-transfected cells were identified by anti-FLAG staining and nucleus were stained by DAPI. Recycled fluorescent signal were analyzed by ImageJ. Briefly, image background was subtracted by rolling ball radius method and then was thresholded. Averaged thresholded fluorescent signal area was obtained for cells.

Statistical analysis

Our power analysis indicated that to detect 20% difference at $\alpha = 0.05$ and $\beta = 0.8$, with < 0.05 probability of false errors using the typical variances we have in our data requires a minimum of 12 samples. No samples were excluded. Data were normally distributed with similar variance between the groups. All the outcomes were independently assessed by investigator without knowledge of treatments. Data are means ± SEM from three independent experiments. Statistical analysis was done with one-way analysis of variance (ANOVA) followed by Tukey's multiple comparison test. *n* represents number of neurons analyzed. $P < 0.05$ was considered to be statistically significant. NS, not significant.

Supplementary Material

Refer to Web version on PubMed Central for supplementary material.

Acknowledgments

This work is partly supported by National Institute of Health grants NS071184 and NS083498 (to X. Zhu) and NS085747 (to X. Wang), by the Clinical and Translational Science Collaborative of Cleveland, UL1TR000439 from the National Center for Advancing Translational Sciences (component of the NIH roadmap for medical research grant no. UL1TR000439; pilot award to X.Z.), by Chinese Overseas, Hong Kong and Macao Scholars Collaborated Research Fund Grant 81228007 to X. Zhu., by the Shanghai Orientalist program (to X.Z.), by the Dr. Robert M. Kohrman Memorial Fund, by the National Natural Science Fund of China (grant no. 81071024, 81171202, 30870879, 81228007 and 81471287; all to J.L.), and the Wellcome Trust (089928 and 085743) and the Medical Research Council (MR/K018299/1) (to P. Cullen). We thank I. Kelmanson (Evrogen) for providing mito-TagBFP and Yisang Yoon (University of Rochemster) for providing DLP1WT and DLP1K38A constructs). Some Parkinson disease tissue samples were obtained from the Harvard Brain Tissue Resource Center, which is supported in part by Public Health Service contract [HHS-NIH-NIDA (MH)-13-265], and from the National Institute of Health Neurobiobank at the University of Maryland.

REFERENCES

1. Chan DC. Fusion and fission: interlinked processes critical for mitochondrial health. Annual review of genetics. 2012; 46:265–287.

2. Yan MH, Wang X, Zhu X. Mitochondrial defects and oxidative stress in Alzheimer disease and Parkinson disease. Free radical biology & medicine. 2013; 62:90–101. [PubMed: 23200807]
3. Burte F, Carelli V, Chinnery PF, Yu-Wai-Man P. Disturbed mitochondrial dynamics and neurodegenerative disorders. Nature reviews. Neurology. 2015; 11:11–24. [PubMed: 25486875]
4. Wang X, et al. Amyloid-beta overproduction causes abnormal mitochondrial dynamics via differential modulation of mitochondrial fission/fusion proteins. Proceedings of the National Academy of Sciences of the United States of America. 2008; 105:19318–19323. [PubMed: 19050078]
5. Chen Y, Dorn GW. PINK1-Phosphorylated Mitofusin 2 Is a Parkin Receptor for Culling Damaged Mitochondria. Science. 2013; 340:471–475. [PubMed: 23620051]
6. Clark IE, et al. Drosophila pink1 is required for mitochondrial function and interacts genetically with parkin. Nature. 2006; 441:1162–1166. [PubMed: 16672981]
7. Narendra D, Tanaka A, Suen DF, Youle RJ. Parkin is recruited selectively to impaired mitochondria and promotes their autophagy. Journal of Cell Biology. 2008; 183:795–803. [PubMed: 19029340]
8. Wang X, et al. LRRK2 regulates mitochondrial dynamics and function through direct interaction with DLP1. Human molecular genetics. 2012; 21:1931–1944. [PubMed: 22228096]
9. Su YC, Qi X. Inhibition of excessive mitochondrial fission reduced aberrant autophagy and neuronal damage caused by LRRK2 G2019S mutation. Human molecular genetics. 2013; 22:4545–4561. [PubMed: 23813973]
10. Irrcher I, et al. Loss of the Parkinson's disease-linked gene DJ-1 perturbs mitochondrial dynamics. Human molecular genetics. 2010; 19:3734–3746. [PubMed: 20639397]
11. Wang X, et al. Parkinson's disease-associated DJ-1 mutations impair mitochondrial dynamics and cause mitochondrial dysfunction. J Neurochem. 2012; 121:830–839. [PubMed: 22428580]
12. Lim KL, Ng XH, Grace LG, Yao TP. Mitochondrial dynamics and Parkinson's disease: focus on parkin. Antioxid Redox Signal. 2012; 16:935–949. [PubMed: 21668405]
13. Vives-Bauza C, et al. Control of mitochondrial integrity in Parkinson's disease. Prog Brain Res. 2010; 183:99–113. [PubMed: 20696317]
14. Sharma M, et al. A multi-centre clinico-genetic analysis of the VPS35 gene in Parkinson disease indicates reduced penetrance for disease-associated variants. Journal of medical genetics. 2012; 49:721–726. [PubMed: 23125461]
15. Vilarino-Guell C, et al. VPS35 mutations in Parkinson disease. American journal of human genetics. 2011; 89:162–167. [PubMed: 21763482]
16. Zimprich A, et al. A mutation in VPS35, encoding a subunit of the retromer complex, causes late-onset Parkinson disease. American journal of human genetics. 2011; 89:168–175. [PubMed: 21763483]
17. Kumar KR, et al. Frequency of the D620N Mutation in VPS35 in Parkinson Disease. Arch Neurol. 2012:1–5.
18. Lesage S, et al. Identification of VPS35 mutations replicated in French families with Parkinson disease. Neurology. 2012; 78:1449–1450. [PubMed: 22517097]
19. Bonifacino JS, Hurley JH. Retromer. Curr Opin Cell Biol. 2008; 20:427–436. [PubMed: 18472259]
20. Burd C, Cullen PJ. Retromer: a master conductor of endosome sorting. Cold Spring Harbor perspectives in biology. 2014; 6
21. Braschi E, et al. Vps35 Mediates Vesicle Transport between the Mitochondria and Peroxisomes. Curr Biol. 2010; 20:1310–1315. [PubMed: 20619655]
22. Soubannier V, et al. A vesicular transport pathway shuttles cargo from mitochondria to lysosomes. Curr Biol. 2012; 22:135–141. [PubMed: 22226745]
23. Sugiura A, McLelland GL, Fon EA, McBride HM. A new pathway for mitochondrial quality control: mitochondrial-derived vesicles. Embo J. 2014
24. Yoon Y, Pitts KR, Dahan S, McNiven MA. A novel dynamin-like protein associates with cytoplasmic vesicles and tubules of the endoplasmic reticulum in mammalian cells. The Journal of cell biology. 1998; 140:779–793. [PubMed: 9472031]

25. Seaman MN. The retromer complex - endosomal protein recycling and beyond. Journal of cell science. 2012; 125:4693–4702. [PubMed: 23148298]
26. Cassidy-Stone A, et al. Chemical inhibition of the mitochondrial division dynamin reveals its role in Bax/Bak-dependent mitochondrial outer membrane permeabilization. Developmental cell. 2008; 14:193–204. [PubMed: 18267088]
27. Roy Chowdhury SK, et al. Impaired adenosine monophosphate-activated protein kinase signalling in dorsal root ganglia neurons is linked to mitochondrial dysfunction and peripheral neuropathy in diabetes. Brain: a journal of neurology. 2012; 135:1751–1766. [PubMed: 22561641]
28. Brand MD, Nicholls DG. Assessing mitochondrial dysfunction in cells. The Biochemical journal. 2011; 435:297–312. [PubMed: 21726199]
29. Merrill RA, et al. Mechanism of neuroprotective mitochondrial remodeling by PKA/AKAP1. PLoS biology. 2011; 9:e1000612. [PubMed: 21526220]
30. Zhu PP, et al. Intra- and intermolecular domain interactions of the C-terminal GTPase effector domain of the multimeric dynamin-like GTPase Drp1. The Journal of biological chemistry. 2004; 279:35967–35974. [PubMed: 15208300]
31. Zhao J, et al. Human MIEF1 recruits Drp1 to mitochondrial outer membranes and promotes mitochondrial fusion rather than fission. Embo J. 2011; 30:2762–2778. [PubMed: 21701560]
32. Liu T, et al. The mitochondrial elongation factors MIEF1 and MIEF2 exert partially distinct functions in mitochondrial dynamics. Experimental cell research. 2013; 319:2893–2904. [PubMed: 23880462]
33. Lucin KM, et al. Microglial beclin 1 regulates retromer trafficking and phagocytosis and is impaired in Alzheimer's disease. Neuron. 2013; 79:873–886. [PubMed: 24012002]
34. McLelland GL, Soubannier V, Chen CX, McBride HM, Fon EA. Parkin and PINK1 function in a vesicular trafficking pathway regulating mitochondrial quality control. The EMBO journal. 2014; 33:282–295. [PubMed: 24446486]
35. Soubannier V, Rippstein P, Kaufman BA, Shoubridge EA, McBride HM. Reconstitution of Mitochondria Derived Vesicle Formation Demonstrates Selective Enrichment of Oxidized Cargo. PLoS ONE. 2012; 7:e52830. [PubMed: 23300790]
36. Neuspiel M, et al. Cargo-Selected Transport from the Mitochondria to Peroxisomes Is Mediated by Vesicular Carriers. Current Biology. 2008; 18:102–108. [PubMed: 18207745]
37. Chan DC. Mitochondrial fusion and fission in mammals. Annu Rev Cell Dev Biol. 2006; 22:79–99. [PubMed: 16704336]
38. Lackner LL, Nunnari JM. The molecular mechanism and cellular functions of mitochondrial division. Biochimica et biophysica acta. 2009; 1792:1138–1144. [PubMed: 19100831]
39. Zunino R, Braschi E, Xu L, McBride HM. Translocation of SenP5 from the nucleoli to the mitochondria modulates DRP1-dependent fission during mitosis. J Biol Chem. 2009; 284:17783–17795. [PubMed: 19411255]
40. Tsika E, et al. Parkinson's disease-linked mutations in VPS35 induce dopaminergic neurodegeneration. Human molecular genetics. 2014; 23:4621–4638. [PubMed: 24740878]
41. McGough, Ian J., et al. Retromer Binding to FAM21 and the WASH Complex Is Perturbed by the Parkinson Disease-Linked VPS35(D620N) Mutation. Current Biology. 2014; 24:1670–1676. [PubMed: 24980502]
42. Follett J, et al. The Vps35 D620N mutation linked to Parkinson's disease disrupts the cargo sorting function of retromer. Traffic (Copenhagen, Denmark). 2014; 15:230–244.
43. Zavodszky E, et al. Mutation in VPS35 associated with Parkinson's disease impairs WASH complex association and inhibits autophagy. Nature communications. 2014; 5:3828.

Methods-only references

44. Wang X, et al. Impaired balance of mitochondrial fission and fusion in Alzheimer's disease. The Journal of neuroscience: the official journal of the Society for Neuroscience. 2009; 29:9090–9103. [PubMed: 19605646]

45. Wang X, Su B, Fujioka H, Zhu X. Dynamin-Like Protein 1 Reduction Underlies Mitochondrial Morphology and Distribution Abnormalities in Fibroblasts from Sporadic Alzheimer's Disease Patients. The American Journal of Pathology. 2008; 173:470–482. [PubMed: 18599615]

46. Fujioka H, Tandler B, Consolo MC, Karnik P. Division of mitochondria in cultured human fibroblasts. Microscopy research and technique. 2013; 76:1213–1216. [PubMed: 24009193]

47. Fujioka H, et al. Decreased Cytochrome c Oxidase Subunit VIIa in Aged Rat Heart Mitochondria: Immunocytochemistry. The Anatomical Record: Advances in Integrative Anatomy and Evolutionary Biology. 2011; 294:1825–1833.

48. Hanaichi T, et al. A stable lead by modification of Sato's method. Journal of electron microscopy. 1986; 35:304–306. [PubMed: 2440973]

Europe PMC Funders Author Manuscripts

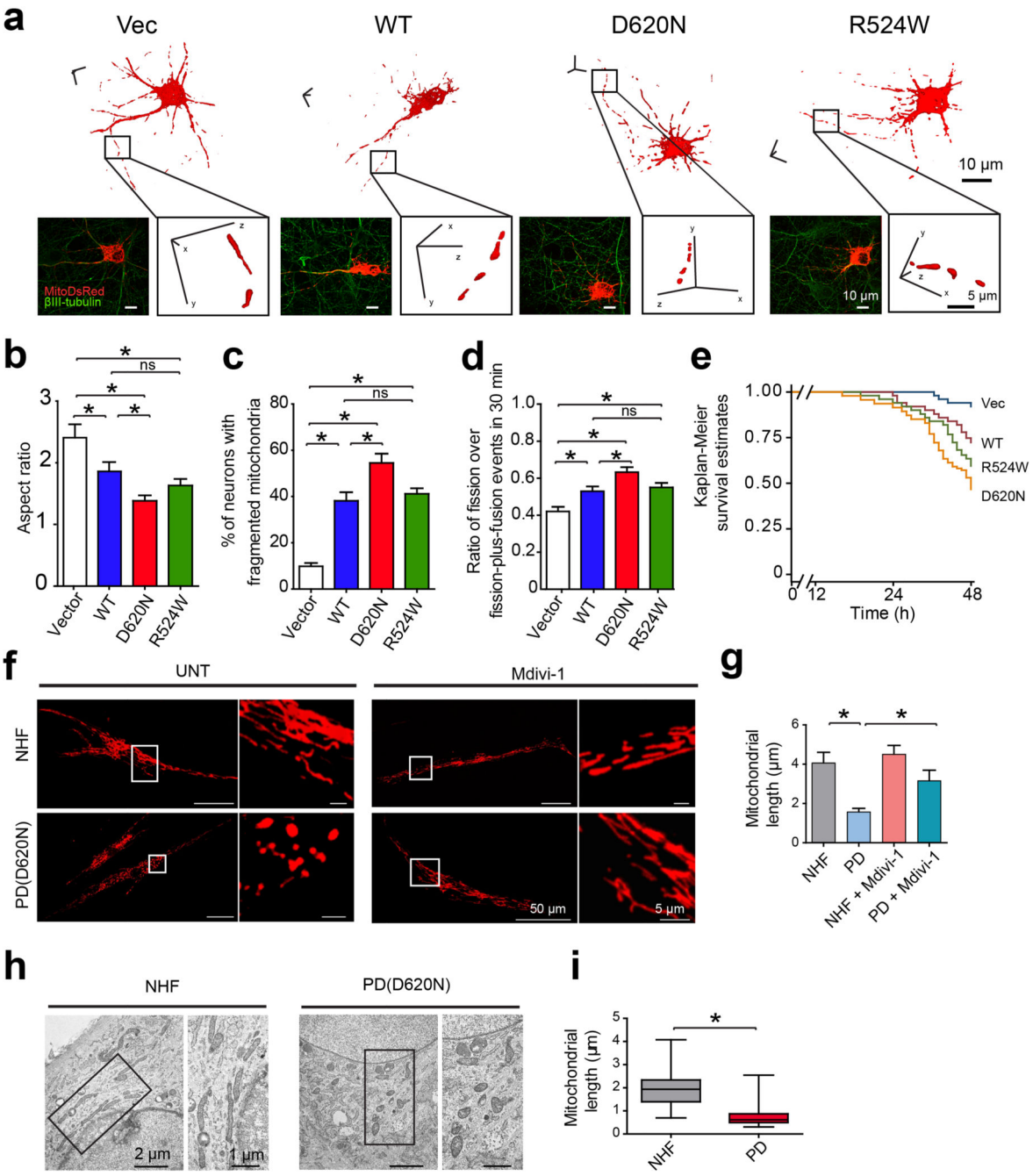

Figure 1. VPS35 regulates mitochondrial dynamics *in vitro*

(**a**) Representative three dimensional (3D) pictures of mitochondria in rat cortical neurons co-transfected with constructs encoding indicated flag-tagged VPS35 and mitoDsRed2. A segment of axon (boxed area) was enlarged. Vec: empty-vector control; WT: wild type. Quantification of mitochondrial aspect ratio (**b**) and percentage of neurons with fragmented mitochondria (**c**) (n = 35, 32, 40, 43 for Vector, WT, D620N and R524W neurons respectively). (**d**) The ratio of fission over fission-plus-fusion events in live neurons expressing VPS35 and mitoDsRed2 (n = 43, 33, 37, 38 for Vector, WT, D620N and R524W

neurons respectively). (**e**) Measurement of neuronal viability in cortical neurons expressing GFP, VPS35 and mitoDsRed2 (n = 51, 46, 55, 51 for Vector, WT, D620N and R524W neurons respectively). Representative confocal images (**f**) and quantification of mitochondrial length (**g**) in fibroblasts from PD subject bearing D620N mutation [PD(D620N)] and normal human fibroblasts (NHFs) with or without mdivi-1 treatment. (n = 34, 44, 27, 53 for NHF, PD, NHF + Mdivi-1 and PD + Mdivi-1 fibroblasts respectively). Representative EM micrographs of mitochondria (**h**) and quantification of mitochondrial length (**i**) in fibroblasts from PD subject with D620N mutation and NHFs. Boxed areas were enlarged to the right of each picture. [A total of 149 and 151 mitochondria from 5 randomly selected NHFs and PD(D620N) fibroblasts were analyzed]. Data are means ± SEM from three independent experiments. Statistics: one-way analysis of variance (ANOVA) followed by Tukey's multiple comparison test. *P < 0.05. ns, not significant.

Europe PMC Funders Author Manuscripts

Europe PMC Funders Author Manuscripts

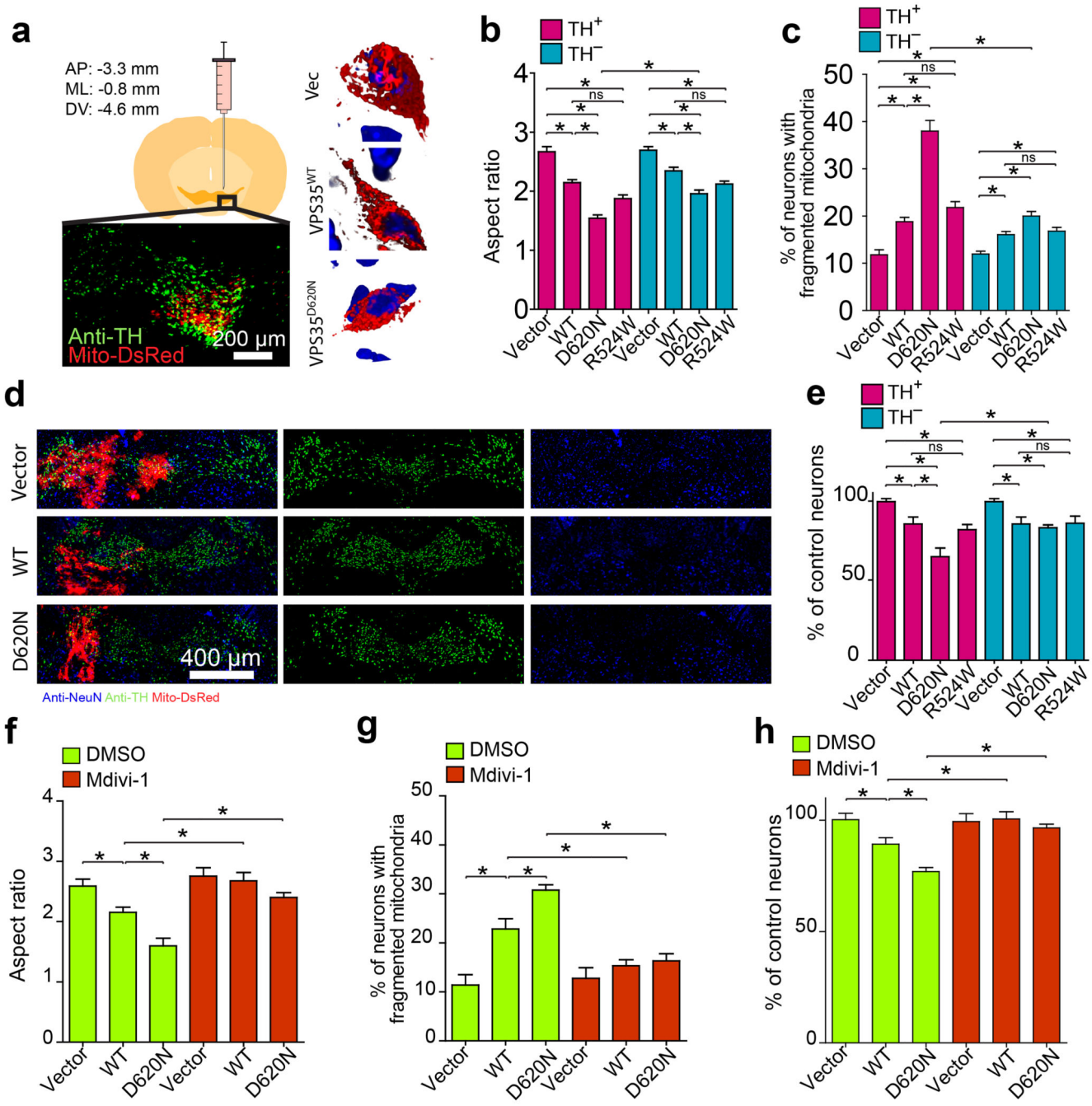

Figure 2. VPS35 regulates mitochondrial dynamics *in vivo*

(**a**) Left: Schematic and representative picture showing the mitochondria (red) in positively transfected TH-positive neurons (green) through stereotactically injection of lentivirus encoding lenti-VPS35-p2a-mitoDsRed2 virus unilaterally into the ventral tegmental area (VTA) of a mouse. Right: Representative 3D image of mitochondria (red) in a TH-positive neuron in the FVB mouse injected with indicated vector (Vec: empty-vector control; $VPS35^{WT}$, wild-type VPS35; $VPS35^{D620N}$, D620N VPS35 mutant). Blue: DAPi. Quantification of mitochondria aspect ratio (**b**), the percentage of neurons with fragmented

Europe PMC Funders Author Manuscripts

mitochondria (**c**) and neuronal loss (**e**) in both TH-positive and TH-negative neurons in FVB mice (2–3 months old) injected with indicated construct (n = 20, 23, 19, 21, 31, 36, 35, 31 for Vector, WT, D620N, R524W TH-positive and TH-negative neurons respectively from three FVB mice/group). (**d**) Representative images of immunofluorescent co-staining of substantia nigra with anti-NeuN (blue) and anti-TH (green) and mitoDsRed2 in FVB mouse injected with indicated construct. (**f-h**) Injected FVB mice were subject to Mdivi-1 treatment and mitochondrial aspect ratio (**f**), the percentage of neurons with fragmented mitochondria (**g**) and neuronal loss (**h**) in TH-positive neurons were analyzed after sacrifice (n = 25, 26, 27, 28, 22, 24, for Vector, WT, D620N, Vector + Mdivi-1, WT + Mdivi-1 and D620N + Mdivi-1 respectively from three mice/group). n represents number of neurons per group. Data are means ± SEM. Statistics: one-way analysis of variance (ANOVA) followed by Tukey's multiple comparison test. $^{*}P < 0.05$. ns, not significant.

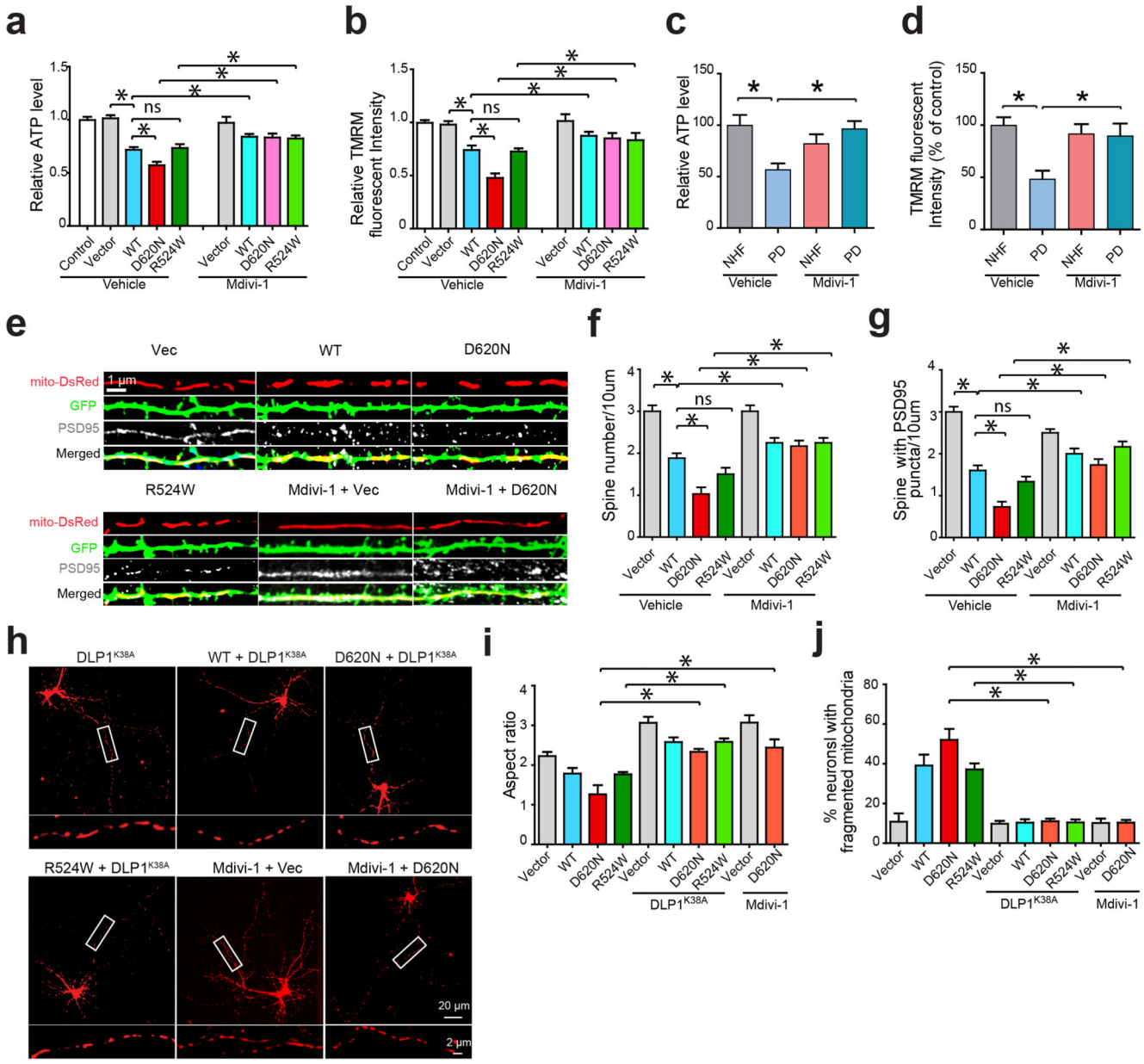

Figure 3. Inhibition of mitochondrial fission alleviates VPS35-induced mitochondrial dysfunction and neuronal deficits

The intracellular levels of ATP (**a,c**) and mitochondrial membrane potential (MMP) (**b,d**) were measured in the stable M17 cell lines (**a**,**b**) and fibroblasts from PD subject bearing VPS35 D620N mutation and NHFs (**c,d**) in the presence or absence of Mdivi-1. Representative images of dendrites (**e**), quantification of dendritic spines (**f**) and PSD95 puncta identified by PSD95 immunostaining (**g**) in primary rat cortical neurons (DIV14) co-transfected with mitoDsRed2 and indicated VPS35 construct and treated with or without Mdivi-1 (n = 24, 23, 25, 28, 22, 27, 25, 25, for vector, WT, D620N, R524W, Vector + Mdivi-1, WT + Mdivi-1, D620N + Mdivi-1 and R524W + Mdivi-1 neurons respectively). In primary cortical neurons co-transfected with mitoDsRed2, dominant-negative DLP1

(DLP1^{K38A}) and indicated VPS35 constructs, representative images of primary cortical neurons (boxed segment of axons enlarged below) (**h**), quantification of mitochondrial aspect ratio in the axon (**i**), and the percentage of neurons with fragmented mitochondria (**j**) were shown (n = 25, 23, 26, 28, 30, 21, 22, 29, 31, 25, for Vector, WT, D620N, R524W, Vector + DLP1 ^{K38A}, WT + DLP1 ^{K38A}, D620N + DLP1^{K38A}, R524W + DLP1^{K38A}, Vector + Mdivi-1 and D620N + Mdivi-1 neurons respectively). n represents number of neurons per group. Data are means ± SEM from three independent experiments. Statistics: one-way analysis of variance (ANOVA) followed by Tukey's multiple comparison test. *P < 0.05. ns, not significant.

Europe PMC Funders Author Manuscripts

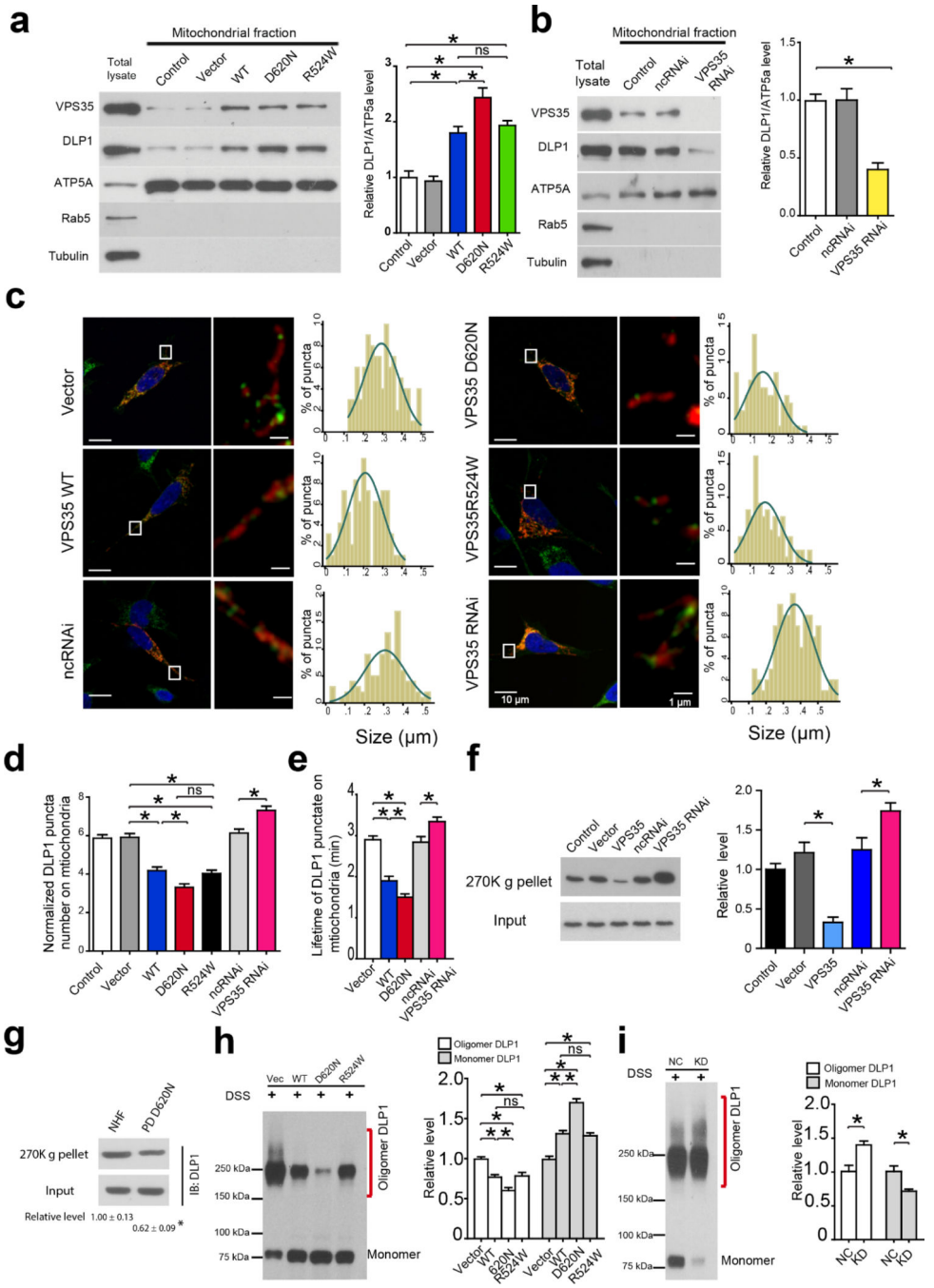

Figure 4. VPS35 promotes the clearance of mitochondrial DLP1 complex

(**a**,**b**) Western blot (left panel) and quantification (right panel) of DLP1 in mitochondrial fraction from indicated M17 stable cell lines. ATP5a, Rab5 and tubulin were used as mitochondrial, endosomal and cytosolic marker respectively. (**c**) Left panels: representative confocal images of DLP1 (green) and mitochondria (red) in mitoDsRed2-transfected M17 cells immunostained with DLP1 (right image is the enlarged image of the boxed area in the left image). Right panels: histogram of mitochondrial DLP1 puncta size (n = 35 for each cell line). (**d**) Quantification of the number of mitochondrial DLP1 puncta in mitoDsRed2-

transfected M17 cells immunostained with DLP1 (n = 35 for each cell line). (**e**) Quantification of the lifetime of mitochondrial GFP-DLP1 puncta in live M17 cells co-transfected with GFP-DLP1 and mitoDsRed2 (n = 25 for each cell line). (**f**) Western blot (left panel) and quantification (right panel) of DLP1 in ultracentrifugation precipitates (270K g pellets) from mitochondrial fraction of indicated M17 stable cell lines exposed to DTME. (**g**) Western blot and quantification of DLP1 in the ultracentrifugation precipitates (270K g pellets) from mitochondrial fraction of fibroblasts from PD subject with D620N mutation and NHFs exposed to DTME. (**h,i**) Western blot of DLP1 (left panel) and quantification (right panel) of the oligomeric and monomeric DLP1 in mitochondrial fraction of M17 cells treated with DSS. n represents number of neurons per group. nc: negative control. Data are means ± SEM from three independent experiments based on three stable M17 clonal lines. Statistics: ANOVA followed by Tukey's multiple comparison test. *P < 0.05. ns, not significant.

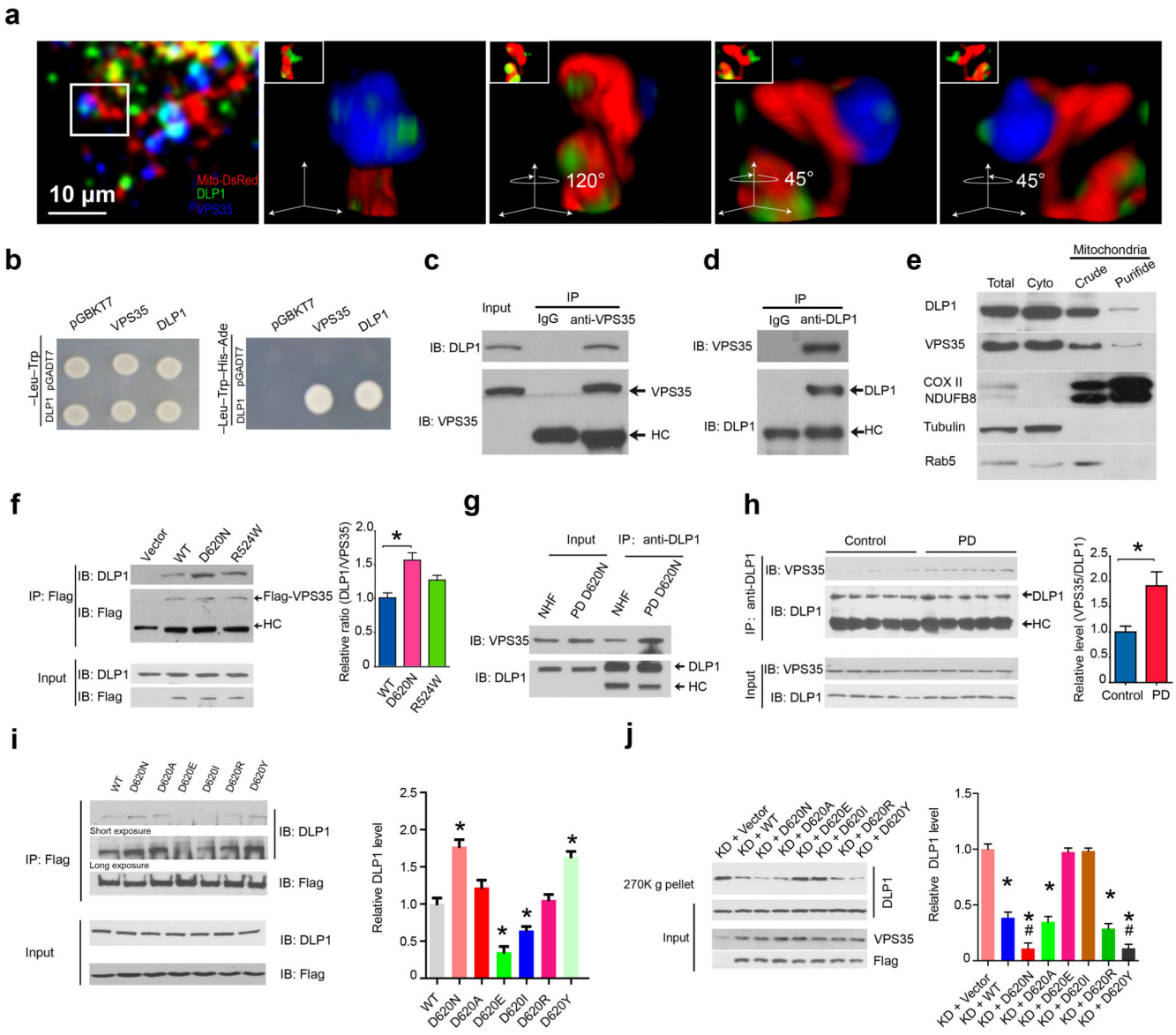

Figure 5. VPS35–DLP1 interaction is key to mitochondrial DLP1 complex turnover

(**a**) Representative 3D images showing the co-localization of endogenous VPS35 and DLP1 on mitochondria in M17 cell transfected with mitoDsRed2 and immunostained with anti-DLP1 and anti-VPS35. Enlargements are the same structure shown at different angles. (**b**) Yeast two-hybrid analysis of VPS35–DLP1 interaction. pGBKT7, pGADT7: empty-vectors. (**c**,**d**) Western blot of DLP1 and VPS35 in VPS35–immunoprecipitates (**c**) and DLP1–immunoprecipitates (**d**) from normal M17 cells. HC: heavy chain. IgG: isotype control antibody without known antigen. (**e**) Western blot of DLP1 and VPS35 in mitochondrial fractions from M17 cells. (**f**) Western blot and quantification of DLP1 in Flag–immunoprecipitates of the highly purified mitochondrial fraction prepared from M17 cells expressing flag-tagged VPS35. (**g**) Western blot of VPS35 and DLP1 in DLP1–immunoprecipitates from fibroblasts from PD subject with D620N mutation and NHFs. (**h**) Western blot and quantification of VPS35 in DLP1–immunoprecipitates from homogenates

Europe PMC Funders Author Manuscripts

of the midbrain of sporadic PD subjects and age-matched controls (n = 5/group). **(i)** Western blot and quantification of DLP1 in Flag–immunoprecipitate from M17 cells expressing indicated flag-tagged VPS35 mutants. **(j)** Western blot and quantification of DLP1 in the ultracentrifugation precipitates (270K g pellets) from mitochondrial fraction of VPS35 KD M17 cell lines expressing indicated flag-tagged VPS35 mutants. Data are means ± SEM from three independent experiments. Statistics: ANOVA followed by Tukey's multiple comparison test. * $P < 0.05$, compared with KD + Vector; # $P < 0.05$ compared with KD + WT.

Europe PMC Funders Author Manuscripts

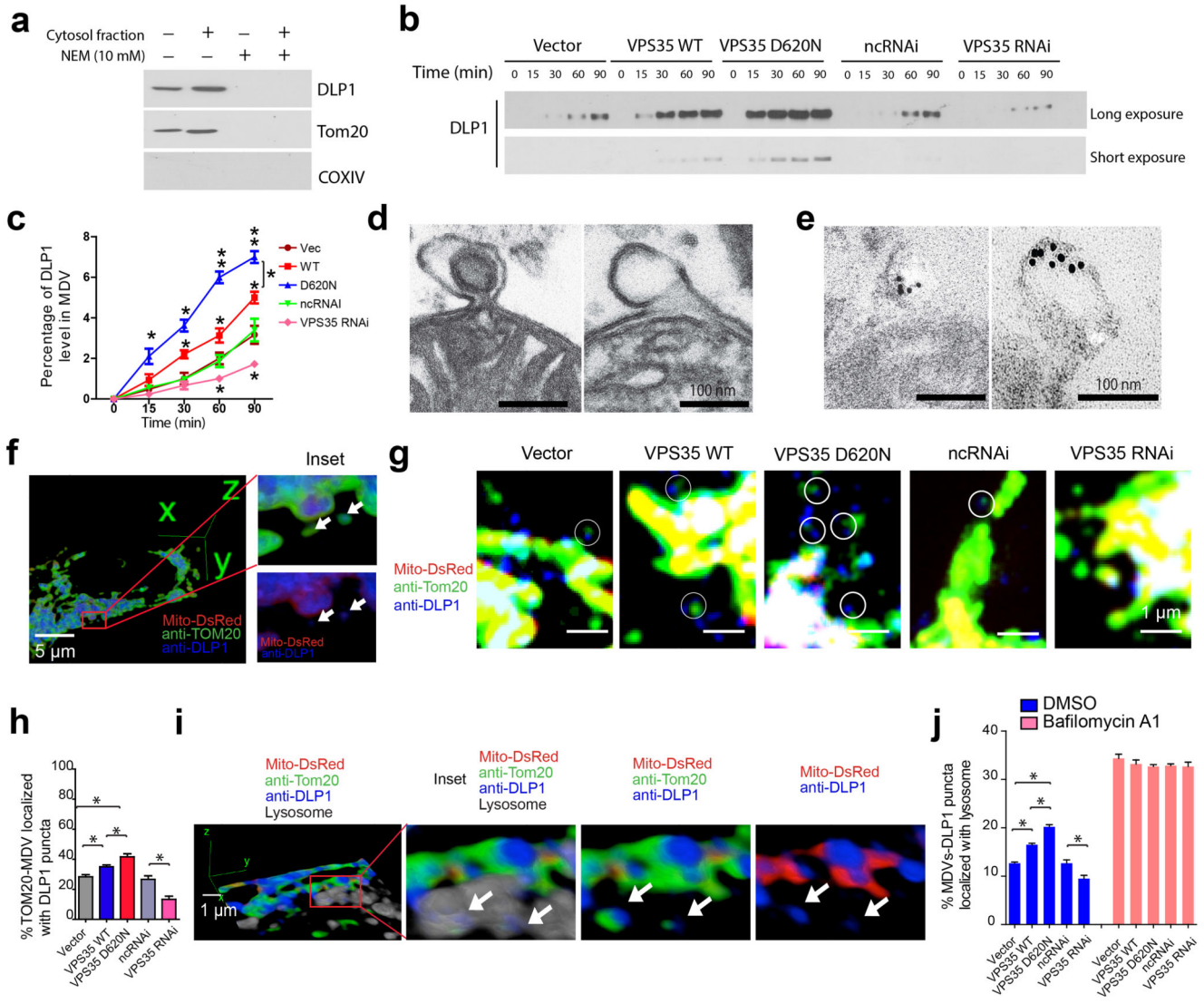

Figure 6. VPS35-retromer mediates mitochondrial DLP1 complex degradation through MDVs–to–lysosome pathway

(**a**) Western blot of DLP1 in *in vitro* reconstituted MDVs. TOM20 and COX IV were used as positive and negative controls for MDVs respectively. Western blot (**b**) and quantification (**c**) of DLP1 in the *in vitro* reconstituted MDVs in the presence of cytosol from indicated M17 cells. (**d**) Representative electron microscopy (EM) micrographs of purified mitochondria highlighted MDVs (both single– and double–membrane) still attached to mitochondrion. (**e**) Immuno-EM micrographs demonstrated the specific labeling of DLP1–immunoreactive gold particles associated with MDVs. (**f**) Representative images showing the co-localization of DLP1 puncta with MDVs (TOM20–positive and mitoDsRed2–negative) in M17 cell. (**g,h**) Representative confocal images (**g**) and quantification (**h**) of the co-localization of DLP1 puncta with MDVs (as highlighted in circles) in stable M17 cell lines. (n = 31, 35, 37, 28, 31 for Vector, WT, D620N, ncRNAi and VPS35 RNAi M17 cells respectively). (**i**) 3D images show the co-localization of DLP1 puncta with MDVs in lysosome in M17 cell. Arrows point to MDVs-associated DLP1 puncta in lysosome. (**j**) Quantification of the percentage of

Europe PMC Funders Author Manuscripts

MDVs associated with DLP1 puncta within lysosome with or without Bafilomycin A1 treatment (n = 33, 28, 35, 37, 31, 31, 35, 36, 27 and 31 for Vector, WT, D620N, ncRNAi and VPS35 RNAi cells with/without Bafilomycin A1 treatment respectively). Data are means ± SEM from three independent experiments. Statistics: ANOVA followed by Tukey's multiple comparison test. * $P < 0.05$.

Europe PMC Funders Author Manuscripts